Short communication

Silicon on conductive self-organized TiO$_2$ nanotubes — A high capacity anode material for Li-ion batteries
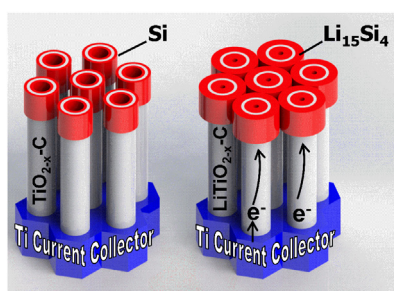
Jassen Brumbarov, Julia Kunze-Liebhäuser[*]

Technische Universität München, Physik Department E19, James-Franck-Str. 1, 85748 Garching, Germany

HIGHLIGHTS

- Lithiation of Si coated self-organized, carburized TiO$_2$ nanotubes.
- Si coated nanotubes show both high cycling stability and specific capacity.
- High rate capability without losing capacity, due to the thin film character of Si.
- Advantages of both active materials can be accessed in a single cell.
- Direct 1D electron transport is enabled without binders or conductive additives.

GRAPHICAL ABSTRACT

ARTICLE INFO

ABSTRACT

The study of high energy density electrode materials is central to the development of Li$^+$-ion batteries. Si is among the most promising anode materials for next generation Li$^+$-ion batteries. Model composite electrodes of self-organized, conductive titania (TiO$_{2-x}$—C) nanotubes coated with silicon (Si) via plasma enhanced chemical vapor deposition (PECVD) are produced and studied in terms of their lithiation/delithiation characteristics. The nanotube array provides direct one dimensional electron transport to the current collector, without the need of adding binders or conductive additives. Both components of the composite can be lithiated delivering 120 μAh cm^{-2} total capacity for a film thickness of 1 μm and a Si loading of $\sim$10 wt.%. 86% capacity retention upon 88 cycles at a rate of C/5 and 60 μAh cm^{-2} total capacity at a rate of 10 C are achieved owing to the low lateral expansion and thus good adhesion of the thin Si coating to the TiO$_{2-x}$—C nanotubes, and due to the formation of a stable solid electrolyte interface (SEI) in ethylene-carbonate (EC), dimethyl-carbonate (DMC), vinylene-carbonate (VC) electrolyte with 1 M LiPF$_6$.

1. Introduction

Due to its high specific capacity of 3580 mAh g^{-1} (Li$_{15}$Si$_4$) [1] at room temperature and low lithiation/delithiation voltage of $\sim$0.5 V vs. Li/Li$^+$, both leading to high energy densities, Si is considered the most promising anode material for next generation Li$^+$-ion batteries. Low Li$^+$ and electronic conductivity however limit the

maximum power output of Si. The high volumetric expansion of Si of up to 280% upon lithiation [2,3], causes fast mechanical degradation of electrodes based on micrometer sized Si particles or films [4]. Additionally, the change in active surface area throughout lithiation/delithiation cycles leads to cracking of the SEI and to its re-formation on freshly exposed Si, which causes SEI thickening, consumption of Li and electrolyte, and consequently to a loss in capacity upon operation. Our approach to overcome these issues is to use a thin Si film of $\sim$10 nm supported on a stable, electronically conducting high aspect ratio surface. Thin Si films are known to

have a superior cycling stability compared to micro particles or films due to their expansion preferentially in direction normal to the film surface avoiding crack formation and delamination [5,6]. Additionally, they provide short diffusion paths for Li^+-ions and electrons allowing for high lithiation/delithiation rates. A drawback of thin films is their low mass per unit area which we compensate by using a support material with a high surface to volume ratio. The use of anodically grown, self-organized TiO_2 nanotubes [7–10] supported on Ti, which directly serves as current collector, and annealed to carbon containing TiO_2 anatase under reducing conditions [11] provides direct one dimensional electron transport towards the current collector and eliminates the need for using conductive carbon to increase the electronic conductivity, which would decrease the electrode's gravimetric capacity. The anatase phase of TiO_2 itself is an active material towards lithium insertion, with a theoretical capacity of 335 mAh g^{-1}, the usually measured capacity of 168 mAh g^{-1} is however used in literature to derive the rate of 1C [12,13]. About 0.6 mol Li can be inserted per mole TiO_2 at 1.78 V vs. Li/Li^+ [14]. Nanotextured anatase TiO_2 can be fully lithiated forming $LiTiO_2$ [15–17].

In this paper, we demonstrate that reversible lithiation takes place in both anatase TiO_2 and Si phases, when self-organized TiO_{2-x}–C nanotubes coated with a Si thin film are used as negative electrode in a half-cell configuration.

2. Experimental

TiO_2 nanotubes were grown electrochemically on mechanically polished (4000P SiC grinding paper) Ti disks (99.6%, Advent) by exposing the polished surface (0.38 cm^2) to an electrolyte containing 50% ethylene glycol by volume (99.5%, Merck) in water (18.2 MΩ cm, Milli-Q, Millipore) and 1 wt.% NH_4F (99.99%, Merck) and by applying an anodic potential of 20 V for 1 h, after a voltage ramp of 1 V s^{-1}. After anodizing, the sample was thoroughly rinsed with deionized water (18.2 MΩ cm, Milli-Q, Millipore) to prevent further etching of the surface. In order to increase the electronic conductivity and to modify the Li insertion properties of the as grown amorphous TiO_2 nanotubes, carbo-thermal annealing was carried out in a horizontal tube furnace. The reactor tube was first purged with 750 sccm Ar for 2 h at room temperature (RT) to remove air. The Ar flow was then reduced to 200 sccm and kept constant until the end of the annealing procedure. Prior to increasing the temperature, 5 sccm acetylene were added to the Ar flow for 3 min. To avoid thermal stress during the temperature increase to 400 °C, the ramping speed was gradually reduced from 10 °C min^{-1} until 200 °C, to 5 °C min^{-1} until 300 °C, and finally 3 °C min^{-1} until 400 °C. After 20 min at 400 °C, 0.1 sccm acetylene was added to the Ar flow for 1 h. The system was then kept for another 280 min at 400 °C to allow for the complete transformation of the nanotubes and then cooled down to RT with 3 °C min^{-1}. PECVD (Oxford Plasmalab 80+) with Ar diluted SiH_4 was used to coat the annealed nanotubes with silicon, at 1 Torr total pressure, with 465 sccm Ar and 35 sccm SiH_4 at 250 °C for 1 min.

Scanning electron microscopy (SEM) (CrossBeam NVision 40, Zeiss) micrographs of TiO_{2-x}–C nanotubes before and after Si deposition were used to determine the volume and therefore mass fraction of deposited Si. Energy Dispersive X-ray Spectroscopy (EDX) (JSM-7500F, JEOL) and X-ray Photoelectron Spectroscopy (XPS) (Specs Phoibos 100 hemispherical electron energy analyzer and a MCD-5 detector) were used ex-situ to qualitatively determine the chemical composition of the electrodes and the oxidation states of their components prior to cycling. The take off angle in XPS measurements was 0 relative to the surface normal and an Al K_α X-ray source (1486.6 eV) without monochromator was used. High resolution spectra were recorded for the Si 2p, Ti 2p, and C 1s
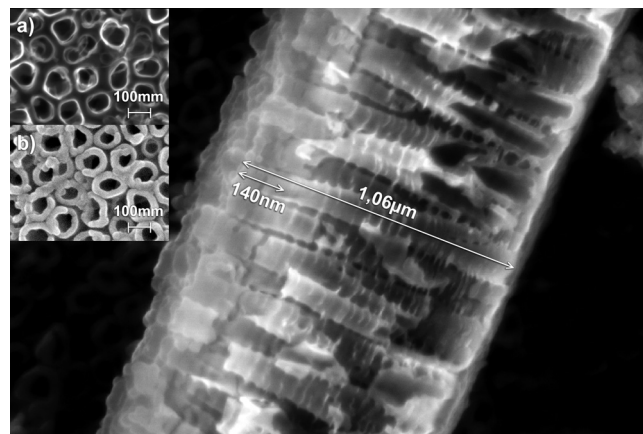

Fig. 1. SEM cross-section of TiO_{2-x}–C nanotubes coated with Si; inset a): top view of non-coated TiO_{2-x}–C nanotubes; inset b): top view of Si-coated TiO_{2-x}–C nanotubes.

regions with a step size of 0.025 eV and a dwell time of 0.5 s. Quantitative analysis was performed using CasaXPS software (version 2.3.14dev38). All spectra were corrected for charging by shifting them to the position of the Ti 2p3/2 peak of TiO_2 at 458.7 eV.

All electrochemical measurements were carried out in a three electrode t-cell with a stainless steel body (Union Tee Tube Fitting, Swagelok). Perfluoralkoxy (PFA, Swagelok) sealing rings and stainless steel rods (1.4404 stainless steel, StahlRING GmbH) were used for contacting the working (WE), counter (CE) and reference (RE) electrodes. The steel rod current collectors for WE and CE were separated from the cell body by a cylinder made of high density polypropylene (HDPP). Lithium foil (99.9%, Alfa Aesar) was used as CE and RE. The electrolyte (SelectiLite battery electrolyte LP 30, Merck) used in all measurements was 1 M $LiPF_6$ in a 1:1 (w/w) mixture of ethylene carbonate (EC) and dimethyl carbonate (DMC) with or without a 2 wt.% vinylene carbonate (VC) additive [18,19]. Two glass fiber (GF) separators (VWR Glass microfibers filter, 691) soaked with electrolyte were used to separate WE and CE at a pressure of 189 kPa. All cells were assembled in an Ar filled glove box (MBraun) with a water and oxygen content below 0.1 ppm. The assembled cells were connected to a potentiostat (VSP, BioLogic) outside the glove box and all experiments were performed at room temperature. All cyclic voltammetry (CV) measurements were performed with a scan rate of 0.05 mV s^{-1} in the potential window from 0.04 to 3.0 V vs. Li/Li^+. Galvanostatic cycling with potential limitation (GCPL) was carried out in the potential window from 0.04 to 3.0 V vs. Li/Li^+ at a constant current of $j_0/10 = 11.2$ μA cm^{-2} corresponding to a lithiation/delithiation rate of ~0.093 C, where the C-rate of 1 C = 120 μA cm^{-2} is derived from the maximal measured capacity of 120 μAh cm^{-2}. The rate capability of the composite was tested at currents $j_0/10, j_0/5, j_0/2, 1j_0, 2j_0$ and $10j_0$. Due to their different masses and specific capacities, the two components of the composite have different lithiation/delithiation C-rates, assuming that both active materials in the composite are lithiated and delithiated subsequently. The C-rates calculated from the measured maximal values of the specific capacities for a constant current density of 11.2 μA cm^{-2} ($=j_0/10$) are 51 mA $g_{composite}^{-1} = 0.09C_{composite}$, 57 mA $g_{TiO2}^{-1} = 0.21C_{TiO2}$ and 478 mA $g_{Si}^{-1} = 0.16C_{Si}$. The C-rates calculated from the theoretical maximum capacities for each component (3580 mAh g_{Si}^{-1}, 168 mAh g_{TiO2}^{-1} and 534 mAh g^{-1} for the composite containing 10.7 wt.% Si) for the same current density (11.2 μA cm^{-2}) are 51 mA $g_{composite}^{-1} = 0.10C_{composite}$, 57 mA $g_{TiO2}^{-1} = 0.34C_{TiO2}$ and 478 mA $g_{Si}^{-1} = 0.13C_{Si}$. The mass of the composite and its components (TiO_{2-x}–C and Si) was calculated
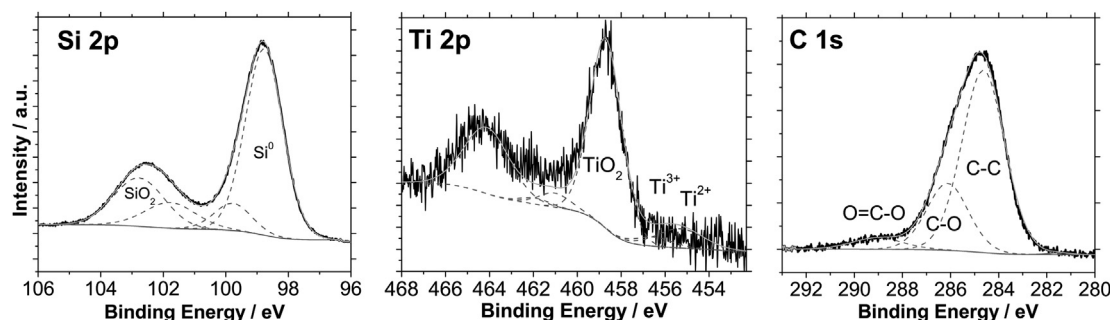
Fig. 2. High resolution XPS spectra of the Si 2p, Ti 2p and C 1s regions of electrodes prior to Li insertion.

using morphological parameters determined by SEM and assuming for TiO_{2-x}–C the density of anatase (3.9 g cm^{-3}) and for the Si coating the density of amorphous Si (2.33 g cm^{-3}). Three concentrical hollow cylinders with flat walls were used to model the composite with the inner and outer cylinders representing the silicon coating. Mean values of nanotube length, wall thickness (at the nanotube top) before and after silicon coating, wall thickness at half length of the nanotubes (without silicon), tube diameter before and after silicon coating, depth of silicon deposit and number of nanotubes per unit geometrical electrode area were used for the mass calculations and their standard deviations for error calculations. The resulting mass of the composite in a representative sample with (0.371 ± 0.006) cm^2 nanotube covered area was (84 ± 14) μg with (75 ± 11) μg TiO_2 and (9 ± 3) μg Si. All potentials given in this work refer to the Li/Li$^+$ scale.

3. Results and discussion

Fig. 1 shows a SEM cross section of Si coated TiO_{2-x}–C nanotubes (Si/TiO_{2-x}–C) and top-views of bare (Fig. 1a) and Si coated (Fig. 1b) nanotubes. Analysis of the SEM micrographs reveals that the Si coating is ∼10 nm thick and that it covers 140 nm of the nanotube top length at both inside and outside walls (see Fig. 1). The mass of deposited Si was estimated to be ∼10 wt.% of the Si/TiO_{2-x}–C composite by calculating its volume fraction determined from the SEM micrographs. An EDX Si map of the composite electrode (not shown) shows that Si is homogeneously distributed over the whole surface, confirming that the thickening of the nanotube walls after PECVD observed by SEM is due to the formation of a Si coating. With EDX, only 7.6 wt.% Si are detected, which is an underestimation arising from the high background signal from the Ti current collector. XPS provides surface sensitive information on the oxidation states of the deposited Si layer (Fig. 2). Silicon and silicon dioxide are identified by their characteristic Si 2p peaks at 98.8 eV and 102.8 eV [18] on the electrodes before Li insertion experiments. The atomic ratio of SiO_2:Si is ∼20:60. Fitting of the Si 2p peak was performed using suboxide peaks according to [20]. The energy separation between successive Si^{n+} species was chosen to follow the expected energy separation of ∼1 eV per chemical state [21]. The high resolution spectra of the Ti 2p and C 1s regions show that the TiO_{2-x}–C mainly consists of TiO_2 with a thin carbon coating. The Ti 2p region was fitted using additional peaks for suboxides according to [22]. However, it has to be noted that due to the small intensity of the Ti 2p signal the background subtraction is imprecise, and the information deduced has a rather qualitative character.

Cyclic voltammetry was used to determine lithiation and delithiation potentials of the Si/TiO_{2-x}–C nanotubes (Fig. 3a). Cyclovoltammograms (CVs) of TiO_{2-x}–C nanotubes were used as reference. Current peaks in the CV curves correspond to the

formation and decomposition of thermodynamically stable lithiated phases or SEI that form at the corresponding potentials. In the high potential region (1.1–3.0 V), the CV of Si/TiO_{2-x}–C shows the characteristic anatase lithiation/delithiation peaks at 1.72 V (A) and 2.03 V (A′), respectively, corresponding to the transition of the Li poor $Li_{0.01}TiO_2$ to the Li rich $Li_{0.55}TiO_2$ phase [12,13]. At low potentials (0.04–1.0 V), two prominent lithiation/delithiation peak pairs 0.25 V (B)/0.48 V (B′) and 0.08 V (C)/0.28 V (C′) appear, that are associated with phase transitions from Si to $Li_{2.5}Si$ and to $Li_{3.75}Si$ [2,5]. Peak B in the first cycle is a double peak with sub peaks at 0.24 and 0.26 V. The presence of peaks B and C in the first cycle indicates that the Si thin film is amorphous prior to lithiation experiments [23–26]. Additionally, three small broad peaks are measured in the first lithiation cycle at 0.36 V (D), 0.49 V (E) and 0.75 V (F), and a broad shoulder is detected upon delithiation from 0.6 V to 1.0 V. In the second CV cycle, peak B becomes a single peak at 0.22 V, and the broad peak F disappears. The peaks D and E become sharp and shift to 0.33 V and 0.46 V, respectively. Their presence can be explained as the formation of additional Li_xSi phases preceding the formation
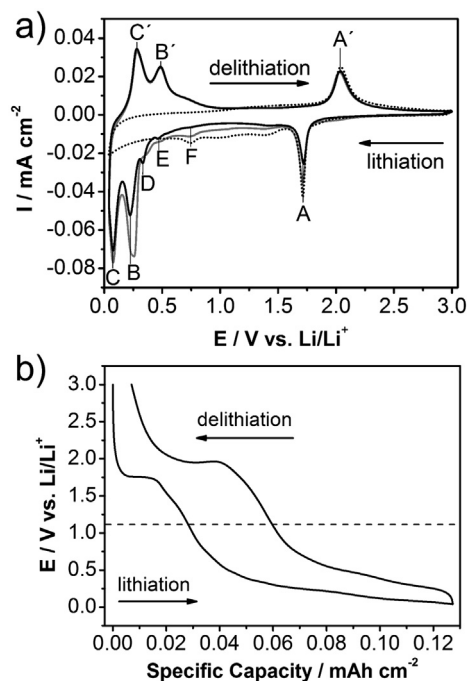

Fig. 3. a) Cyclic voltammograms of Si/TiO_{2-x}–C (solid gray line: 1st cycle, solid black line: 2nd cycle) and TiO_{2-x}–C nanotubes (broken line), scan rate: 0.05 mV s^{-1}, b) galvanostatic charge/discharge curve (first cycle after CV) of Si/TiO_{2-x}–C nanotubes in 1 M LiPF$_6$ in 1:1 EC:DMC with 2 wt% vinylene carbonate (VC).
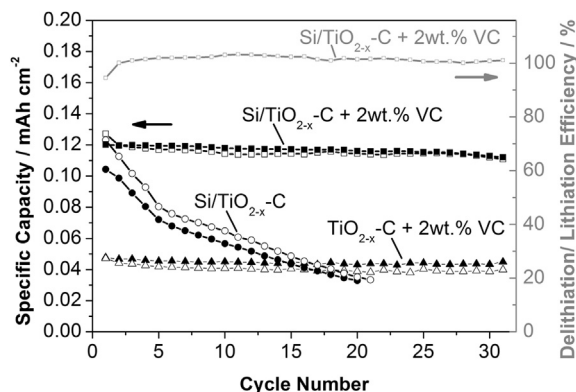
Fig. 4. Specific capacity (black curves) and current efficiency (gray curve) versus cycle number at 11 μA cm^{-2} ($\sim$C/10) for Si/TiO$_{2-x}$–C (with and without 2 wt% VC) and TiO$_{2-x}$–C nanotubes in 1 M LiPF$_6$ in 1:1 EC:DMC. Lithiation: open symbols, delithiation: closed symbols.

Fig. 6. Specific capacity and capacity retention versus cycle number at different constant currents expressed as fractions of j_0, with $j_0 = 112$ μA cm^{-2} (0.93C) of Si/TiO$_x$–C nanotubes in 1 M LiPF$_6$ in 1:1 EC:DMC with 2 wt% VC. Lithiation: open symbols, delithiation: closed symbols.

of Li$_{2.5}$Si. In the reference CV of TiO$_{2-x}$–C, a peak at 0.75 V is detected, which shows that peak F of Si/TiO$_{2-x}$–C must be related to the reduction of VC containing electrolyte in the first lithiation cycle [27].

Lithiation and delithiation capacity (Fig. 3b), cycling stability (Figs. 4 and 5) as well as rate capability (Fig. 6) were measured under galvanostatic conditions. The lithiation curve depicted in Fig. 3b shows two distinct regions corresponding to the two active materials in the composite. The anatase region is prominent from 3.0 V to 1.1 V with one plateau at 1.77 V corresponding to the phase transition of the Li-poor (Li$_{0.01}$TiO$_2$) to the Li-rich phase (Li$_{0.55}$TiO$_2$), and the silicon region from 1.1 V to 0.04 V with multiple slope changes corresponding to the peaks observed in the CV measurements. The fact that the delithiation plateau in the anatase region is larger than its lithiation counterpart compensating for the small delithiation plateau in the silicon region for the total delithiation capacity indicates that Si and TiO$_2$ are not performing independently. It is very likely that the interface between the two active materials plays a crucial role for the lithiation mechanism, which will be investigated separately. It is noteworthy that the silicon region delivers 56% of the total capacity of the composite that contains $\sim$10 wt. % Si only. Using the calculated masses (and their deviations) of the composite and its components, the gravimetric capacity of the composite is determined as 556 mAh g^{-1} with a deviation interval of [478; 664] mAh g^{-1}, the gravimetric capacity of TiO$_{2-x}$–C is 273 mAh g^{-1} [240; 318] mAh g^{-1}, and that of Si 2960
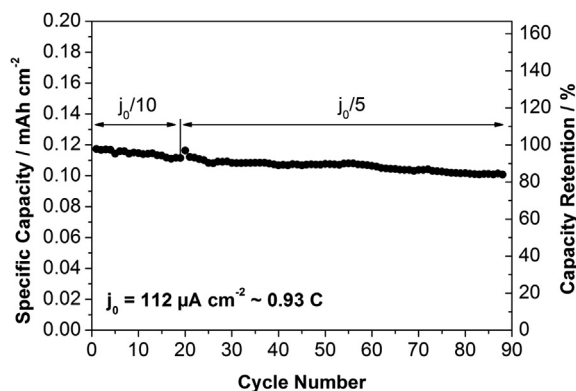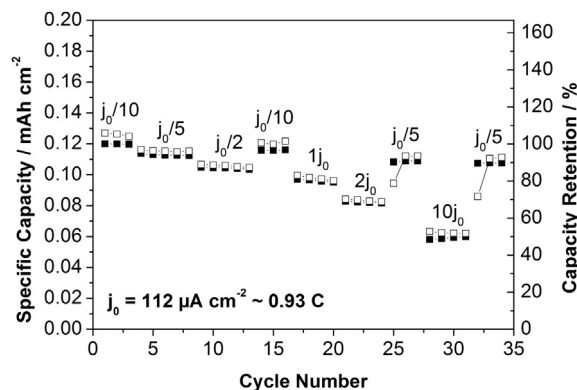

Fig. 5. Specific delithiation capacity and capacity retention versus cycle number at a constant current of 22.4 μA cm^{-2} ($\sim$0.19C) for Si/TiO$_x$–C nanotubes in 1 M LiPF$_6$ in 1:1 EC:DMC with 2 wt% VC.

mAh g^{-1} [2184; 4583] mAh g^{-1}. A lithiation degree of more than 0.55 mol Li per TiO$_2$ is reached in the TiO$_{2-x}$–C nanotubes since even the lower capacity limit of 240 mAh g^{-1} for TiO$_{2-x}$–C is higher then the 168 mAh g^{-1} capacity corresponding to the formation of Li$_{0.55}$TiO$_2$. However, the uncertainties of the gravimetric capacities, induced by non-accurate determination of the active masses, are high due to the small dimensions of nanotubes and Si coating, and due to the correspondingly high relative error of the morphological parameters. This makes the determination of the lithiation degree of the Si coating by comparison of measured with theoretical values for gravimetric capacities of lithiated phases insignificant. Due to its low error of <2%, the areal capacity is chosen to represent the experimental data rather than gravimetric capacity. Fig. 4 depicts the measured specific areal capacity as a function of cycle number for the TiO$_{2-x}$–C nanotubes with and without Si coating in electrolyte with and without VC. In the electrolyte containing 2 wt.% VC additive, the nanotubular Si/TiO$_{2-x}$–C composite shows a delithiation capacity of (120 ± 2) μAh cm^{-2} in the first cycle (after the CV) that decreases to 110 μAh cm^{-2} or 93% after 30 cycles and 86% after 88 cycles (Fig. 5), which is 2.4 times higher than the capacity of a TiO$_{2-x}$–C nanotube electrode without Si coating measured under the same conditions (see Fig. 4). The delithiation/lithiation efficiency of the Si/TiO$_{2-x}$–C electrode increases from 94% in the first cycle to 100% in the second cycle and remains at that level until the end of the measurement. In contrast, a Si/TiO$_{2-x}$–C electrode cycled in electrolyte without VC retains only 32% of its capacity in the first 20 cycles (see Fig. 4). Its delithiation/lithiation efficiency (not shown) changes from 85% in the first to 94% in the 20th cycle without reaching steady state. Since the VC additive is the only difference in the two measurements, the very low initial efficiency in the case where no additive was used can be attributed to a massive formation of unstable SEI. The TiO$_{2-x}$–C nanotube electrode shows a noticeably higher delithiation than lithiation capacity over 30 cycles, this effect is also visible at Si/TiO$_{2-x}$–C, but much less pronounced. The origin of this might be related to the SEI formation process. In cyclic voltammograms of TiO$_{2-x}$–C and of Si/TiO$_{2-x}$–C nanotubes in LiPF$_6$ containing EC/DMC + VC electrolyte, we see SEI formation at 0.75 V (see Fig. 3a, peak F). After the initial SEI formation cycle at TiO$_{2-x}$–C electrodes, the deintercalation peak of anatase shifts from 2.04 V (first cycle) to 2.12 V after 11 cycles. With cycling a shoulder in the deintercalation peak develops that is located at $\sim$2.17 V after 11 cycles. The charge under the peak increases with cycling and exceeds that of the intercalation peak (not shown). This effect might be due to oxidative processes at the nanotube surface covered with electrolyte decomposition products

after the initial lithiation cycle, such as ethylene, carbon monoxide and dioxide, and methane, as described in Ref. [27], where also higher anodic currents are shown on composite graphite anodes in $LiPF_6/EC + DMC + 2$ wt.% VC. Future work will study in more detail the SEI formation and related processes at Ti_{2-x}–C and at Si thin film electrodes. Fig. 5 shows the specific areal capacity of the Si/TiO_{2-x}–C nanotubes over 88 cycles in VC containing electrolyte. The first 19 cycles are performed at a constant current of $j_0/10$ ($\sim$C/10), cycles 20 to 88 at $j_0/5$ ($\sim$C/5). The higher capacity at cycle 20 originates from switching to the higher current ($j_0/5$) during the measurement. No significant change in capacity is observed upon changing the constant current from $j_0/10$ to $j_0/5$, and a high capacity of 101 µAh cm^{-2} (86%) is retained from the initial 117 µAh cm^{-2} after 88 cycles. Galvanostatic lithiation/delithiation was also performed at different constant currents (Fig. 6), in order to study the rate capability of the composite. The maximum capacity of 120 µAh cm^{-2} is reached at a rate of $j_0/10$ ($\sim$C/10) decreasing gradually with increasing rate to 112 µAh cm^{-2} (93%) at $j_0/5$ ($\sim$C/5), 104 µAh cm^{-2} (87%) at $j_0/2$ ($\sim$C/2), 95 µAh cm^{-2} (79%) at $1j_0$ ($\sim$1 C), 82 µAh cm^{-2} (68%) at $2j_0$ ($\sim$2 C) and to 60 µAh cm^{-2} (50%) at $10j_0$ ($\sim$10 C). Going back with the rate to $j_0/10$ after cycling at $j_0/2$ returns 116 µAh cm^{-2} (97%), going back to $j_0/5$ after $2j_0$ returns 109 µAh cm^{-2} (97% of the first $j_0/5$ scan), and going back to $j_0/5$ after $10j_0$ returns 108 µAh cm^{-2} (96% of the first $j_0/5$ scan), which is almost identical to the capacity retention of 93% observed after cycling at a constant rate of C/10 (Fig. 4). This finding suggests that there is no accelerated degradation of the composite when cycled at rates up to 10 C.

4. Conclusions

Good cycling stability, rate capability and high specific capacity of Si coated, self-organized, and electronically conductive TiO_{2-x}–C nanotubes is achieved through minimizing the Si film thickness to $\sim$10 nm, which leads to a reduction of mechanical stress and of variation in active surface area upon lithiation/delithiation and to an improvement of Li$^+$-ion and electron diffusivity. The low Si film thickness is compensated by the high surface area (surface area = 28 × electrode area) of the TiO_{2-x}–C nanotube support. For a production of high capacity Si/TiO_{2-x}–C anodes, complete coating of the TiO_{2-x}–C nanotubes with Si should be achieved, which we are currently working on by using electrochemical Si deposition methods. Using anatase TiO_{2-x}–C as support material for Si, which is also active for Li insertion, additionally increases the total capacity of the composite. Moreover, the introduction of a second potential window for lithiation makes new applications possible where the advantages of both active materials can be accessed in a single cell. The specially designed nanostructure of the electrode ensures very short diffusion paths for Li$^+$-ions and electrons, enabling high rate lithiation/delithiation of both components of the composite at room temperature. High rates can be applied without losing capacity, most likely due to the low lateral expansion and thus good adhesion of the thin Si coating and the formation of a stable solid electrolyte interface (SEI). The addition of VC to the electrolyte plays a crucial role for improving cycling stability, most likely due to an improvement of the SEI properties. Binders and conductive additives are not required, since direct one dimensional electron transport towards the Ti current collector is enabled by the carbon coating of the TiO_{2-x}–C nanotubes.

Acknowledgments

References

[1] M.N. Obrovac, L. Christensen, Electrochem. Solid-State Lett. 7 (2004) A93–A96.
[2] J.W. Wang, Y. He, F. Fan, X.H. Liu, S. Xia, Y. Liu, C.T. Harris, H. Li, J.Y. Huang, S.X. Mao, T. Zhu, Nano Lett. 13 (2013) 709–715.
[3] S.D. Beattie, D. Larcher, M. Morcrette, B. Simon, J.-M. Tarascon, J. Electrochem. Soc. 155 (2008) A158–A163.
[4] S. Bourderau, T. Brousse, D.M. Schleich, J. Power Sources 81-82 (1999) 233–236.
[5] T.L. Kulova, A.M. Skundin, Y.V. Pleskov, E.I. Terukov, O.I. Kon'kov, J. Electroanal. Chem. 600 (2007) 217–225.
[6] S. Ohara, J. Suzuki, K. Sekine, T. Takamura, J. Power Sources 136 (2004) 303–306.
[7] V. Zwilling, M. Aucouturier, E. Darque-Ceretti, Electrochim. Acta 45 (1999) 921–929.
[8] D.J. LeClere, A. Velota, P. Skeldon, G.E. Thompson, S. Berger, J. Kunze, P. Schmuki, H. Habazaki, S. Nagata, J. Electrochem. Soc. 155 (2008) C487–C494.
[9] S. Leonardi, A.L. Bassi, V. Russo, F. Di Fonzo, O. Paschos, T.M. Murray, H. Efstathiadis, J. Kunze, J. Phys. Chem. C (2012) 384–392.
[10] P. Roy, S. Berger, P. Schmuki, Angew. Chem. Int. Ed. Engl. 50 (2011) 2904–2939.
[11] R. Hahn, F. Schmidt-Stein, J. Salonen, S. Thiemann, Y. Song, J. Kunze, V.-P. Lehto, P. Schmuki, Angew. Chem. Int. Ed. Engl. 48 (2009) 7236–7239.
[12] M. Mancini, P. Kubiak, J. Geserick, R. Marassi, N. Hüsing, M. Wohlfahrt-Mehrens, J. Power Sources 189 (2009) 585–589.
[13] D. Bresser, E. Paillard, E. Binetti, S. Krueger, M. Striccoli, M. Winter, S. Passerini, J. Power Sources 206 (2012) 301–309.
[14] T. Ohzuku, T. Kodama, T. Hirai, J. Power Sources 14 (1985) 153–166.
[15] W.J.H. Borghols, D. Lützenkirchen-Hecht, E.R.H. van Eck, F.M. Mulder, M. Wagemaker, Phys. Chem. Chem. Phys. PCCP 11 (2009) 5742–5748.
[16] M. Wagemaker, W.J.H. Borghols, F.M. Mulder, J. Am. Chem. Soc. 129 (2007) 4323–4327.
[17] J. Brumbarov, P. Vivek, J. Kunze-Liebhäuser, in preparation.
[18] L. Chen, K. Wang, X. Xie, J. Xie, J. Power Sources 174 (2007) 538–543.
[19] I.A. Profatilova, C. Stock, A. Schmitz, S. Passerini, M. Winter, J. Power Sources 222 (2013) 140–149.
[20] F. Yubero, A. Barranco, J.A. Mejias, J.P. Espinos, A.R. Gonzalez-Elipe, Surf. Sci. 458 (2000) 229–238.
[21] F.G. Bell, L. Ley, Phys. Rev. B 37 (1988) 8383–8393.
[22] C. Rüdiger, F. Maglia, S. Leonardi, M. Sachsenhauser, I.D. Sharp, O. Paschos, J. Kunze, Electrochim. Acta 71 (2012) 1–9.
[23] C. Pereira-Nabais, J. Świątowska, A. Chagnes, F. Ozanam, A. Gohier, P. Tran-Van, C.-S. Cojocaru, M. Cassir, P. Marcus, Appl. Surf. Sci. 266 (2013) 5–16.
[24] V. Baranchugov, E. Markevich, E. Pollak, G. Salitra, D. Aurbach, Electrochem. Commun. 9 (2007) 796–800.
[25] M. Green, E. Fielder, B. Scrosati, M. Wachtler, J.S. Moreno, Electrochem. Solid-State Lett. 6 (2003) A75–A79.
[26] L.B. Chen, J.Y. Xie, H.C. Yu, T.H. Wang, J. Appl. Electrochem. 39 (2009) 1157–1162.
[27] H. Ota, Y. Sakata, A. Inoue, S. Yamaguchi, J. Electrochem. Soc. 151 (2004) A1659.